

**A Nondestructive Device for Measuring the
Thickness of Concrete Pavement**

Research Report 0-4414-2

**Performed in Cooperation with the
Texas Department of Transportation
and the Federal Highway Administration
Project 0-4414-2**

By

**Richard Liu
Jing Li
Xuemin Chen
Huichun Xing
Renyue Liang**

**Subsurface Sensing Laboratory
Department of Electrical and Computer Engineering
University of Houston**

December 2005

1. Report No. FHWA/TX-04/0-4414-2		2. Government Accession No.		3. Recipient's Catalog No.	
4. Title and Subtitle A Nondestructive Device for Measuring the Thickness of Concrete Pavement				5. Report Date April 2002	
				6. Performing Organization Code	
7. Author(s) Richard Liu, Jing Li, Xuemin Chen, Huichun Xing, Renyue Liang				8. Performing Organization Report No. Report 0-4414-2	
9. Performing Organization Name and Address Department of Electrical and Computer Engineering University of Houston 4800 Calhoun Rd. Houston, TX 77204-4793				10. Work Unit No.	
				11. Contract or Grant No. Project 0-4414	
12. Sponsoring Agency Name and Address Texas Department of Transportation Research and Technology Implementation Office P.O. Box 5080 Austin, TX 78763-5080				13. Type of Report and Period Covered Final Report December 1, 2000 – November 31, 2001	
				14. Sponsoring Agency Code	
15. Supplementary Notes Project performed in cooperation with the Texas Department of Transportation and the Federal Highway Administration. URL: http://subsurface.ee.uh.edu/documents/0-4414-2.pdf					
16. Abstract: In research Project 0-4172 "Development of a Thickness Measurement Device for Steel Reinforced Concrete Pavement" provided a rudimentary radar system that was able to measure concrete pavement thickness, for pavement without steel reinforcement, up to 18 inches. In this project, the GPR system developed in Project 0-4172 is further improved to measure concrete thickness with steel reinforcement. Prototype GPR system was manufactured and an efficient thickness computation algorithm is implemented. The developed GPR thickness measurement system was both lab and field-tested. GPR system is mounted on a pushcart for easy operation. There are two display screens mounted on the GPR: one displays the GPR traces in colour map format and the other displays thickness and distance in text format. Field tests were done on the construction site of US Highway 59 south in Sugar Land area. Field-tested results showed that the GPR is able to measure steel reinforced concrete up to 16 inches with an average error of 2%. In the mean time, the location and diameter of the steel rebars can be obtained. This system also measures the dielectric constant of the concrete automatically. The dielectric constant may be useful in estimating concrete maturity.					
17. Key Words Pavement thickness, Dielectric constant, weak signal extraction, TEM horn antenna, Pulse generator			18. Distribution Statement No restrictions. This document is available to the public through National Technical Information Service, Springfield, Virginia, 22161, www.ntis.gov		
19. Security Classif. (of this report) Unclassified		20. Security Classif. (of this page) Unclassified		21. No. of Pages 39	22. Price

**A Nondestructive Device for Measuring the Thickness of Concrete
Pavement**

by

Richard Liu, Jing Li, Xuemin Chen, Huichun Xing and Renyue Liang

Research Report 0-4414-2

Project Number: FHWA/TX-04/0-4414

Project title: Development of a Thickness Measurement Device for Steel Reinforced
Concrete Pavement

Performed in Cooperation with the
Texas Department of Transportation
and the
Federal Highway Administration

by the

Subsurface Sensing Laboratory
Department of Electrical and Computer Engineering
University of Houston

December 2005

DISCLAIMERS

The contents of this report reflect the views of the authors, who are responsible for the facts and the accuracy of the data presented herein. The contents do not necessarily reflect the official view or policies of the Federal Highway Administration (FHWA) or the Texas Department of Transportation (TxDOT). This report does not constitute a standard, specification, or regulation.

University of Houston
4800 Calhoun Rd.
Houston, TX 77204

ACKNOWLEDGMENTS

We greatly appreciate the financial support from the Texas Department of Transportation that made this project possible. The support of the project director, Dr. Moon Won and program coordinator Ed Oshinski is also very much appreciated. We also thank the Project Monitoring Committee member Dr. German Claros.

Table of Contents

CHAPTER 1: INTRODUCTION.....	1
1.1 BACKGROUNDS AND OVERVIEW	1
CHAPTER 2: HARDWARE IMPROVMENTS.....	3
2.1 INCREASING GPR’S SAMPLING POINTS.....	3
2.2 REDUCING DIRECT COUPLINGS	5
2.3 INCREASING DYNAMIC RANGE	7
2.4 DISTANCE MEASUREMENTS AND DISPLAY DEVICE.....	8
2.5 LCD DISPLAY.....	9
CHAPTER 3: REFLECTED SIGNAL EXTRACTION USING THE SHORT TIME FOURIER TRANSFORM (STFT).....	11
3.1 INTRODUCTION TO STFT.....	11
3.2 STFT COMPUTATION	12
3.2.1 VERIFICATION OF THE ALGORITHM.....	12
3.2.2 WINDOW WIDTH SELECTION.....	13
3.3 STFT RESULT ANALYSIS	15
3.4 APPLICATION PROCEDURES OF STFT	20
CHAPTER 4: REBAR PROCESSING	21
4.1 REBAR’S EFFECTS IN PAVEMENT MEASUREMENT	21
4.2 MEARING METHODOLOGY ON REBAR-REINFORCED PAVEMENT	23
CHAPTER 5: FIELD MEASUREMENT RESULTS.....	27
5.1 MEASURED RESULTS ON HIGHWAY PAVEMENT WITH STEEL REBAR	27

CHAPTER 6: CONCLUSIONS AND RECOMMENDATIONS.....	31
6.1 CONCLUSIONS.....	31
6.2 RECOMMENDATIONS.....	32

List of Figures

Figure 1.1 Block diagram of GPR radar for thickness measurement	1
Figure 2.1 Measured signals using different sampling points	4
Figure 2.2 Ferrite filters applied on cables	5
Figure 2.3 Effects of filtering using Ferrite filters, (a) with and (b) without filters	6
Figure 2.4 Signals measured by different radar dynamic range	7
Figure 2.5 Pulses generated by the encoder.....	8
Figure 2.6 The LCD display is clearly seen even under direct sunlight.....	9
Figure 2.7 The Finalized GPR thickness measurement system.....	10
Figure 3.1 Data sequence noischir (n) and its dominant frequency.....	13
Figure 3.2 The time-domain signal and its dominating frequency at different c , $c=0.015$, 0.02 and 0.025 respectively	14
Figure 3.3 STFT results of may109inch.dat from point 42 to point 56.....	17
Figure 3.4 STFT results of may10groundfre.dat from point 42 to point 56.....	19
Figure 4.1 Rebar Structure in highway pavement	21
Figure 4.2 Radar's polarization.....	22
Figure 4.3 Rebar's reflection versus its relative positions.....	23
Figure 4.4 Multi-trace chart on highway pavement.....	24
Figure 4.5 Traces measured over and off the rebar	25
Figure 5.1 Field test of the developed thickness radar over new pavement with steel rebar (Picture taken by Ed Oshinsky).....	27
Figure 5.2. Cross sectional view of the concrete pavement used to test the GPR thickness measurement system. Longitudinal rebar is not shown in this figure.....	28
Figure 5.3 GPR image obtained on the pavement during the field test	29
Figure 5.4 Comparison of the radar-measured thickness and ruler-measured thickness....	30

List of Tables

Table 4.1 Rebar's reflections in different orientation.....	22
Table 4.2 Rebar's reflections at different positions	23
Table 5.1 Average measurement errors by GPR	29

CHAPTER 1: INTRODUCTION

1.1 BACKGROUND AND OVERVIEW

In the previous project (No. 0-4172), a prototype of GPR radar for the measurement of concrete thickness was developed. The block diagram of the radar system is shown in [Figure 1.1](#).

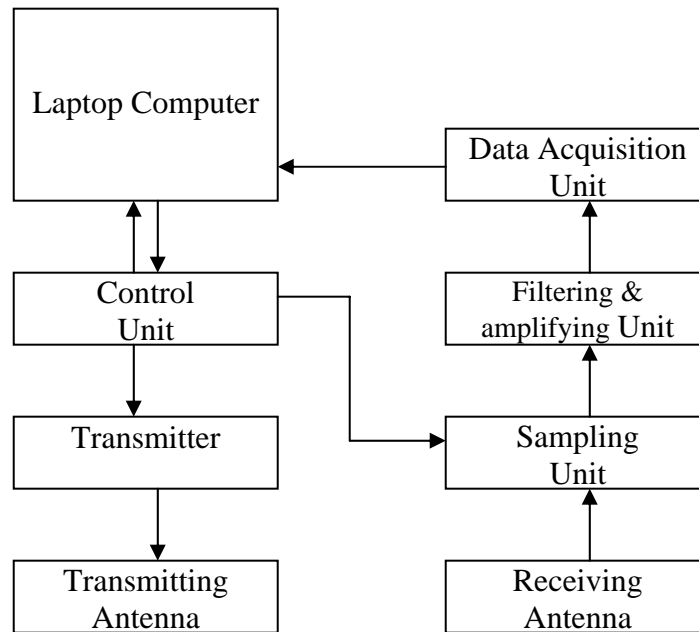


Figure 1.1 Block diagram of GPR radar for thickness

The GPR system is mainly composed of eight parts: a transmitter, a transmitting antenna, a receiving antenna, a sampling unit, a filtering and amplifying unit, a data acquisition unit, a control unit and a laptop computer. The computer is used to control the GPR system and process the sampled data. When the control unit receives a command from the computer, it triggers the transmitter to emit a short pulse wave into the space via the transmitting antenna. At the same time, the control unit also sends a command to the sampling unit to get the unit ready for the incoming reflected signals. The transmitted wave from the transmitting antenna will propagate in all directions in the space, and part of it will penetrate into the pavement. When the penetrated wave

encounters the subsurface interface, it will be reflected back and be picked up by the receiving antenna. There is also a part of the transmitted wave propagating directly from the transmitting antenna to the receiving antenna or from the transmitting antenna to the pavement surface and then bouncing back to the receiving antenna, which is called the direct wave. Hence the received signal mainly consists of two parts, the direct wave and the subsurface reflected wave. By processing the received signals, the thickness of the pavement can be obtained. The developed radar was able to measure the concrete pavement with a thickness up to 16.5 inches without steel rebars, but the measured data was not accurate enough in the presence of the steel rebars.

In order to obtain more accurate measurement of the pavement thickness in the presence of steel rebars, both hardware and software of the GPR system are greatly improved in this research. The hardware and software improvements and the measured results on test sites are presented in this report.

CHAPTER 2: HARDWARE IMPROVEMENTS

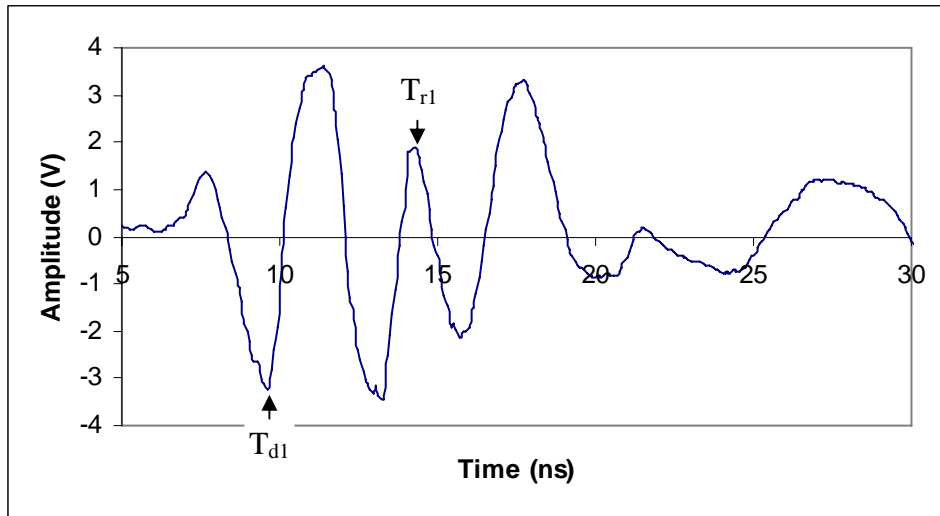
The key problem in measuring the thickness of concrete pavement is to obtain clear signals reflected from the bottom of the pavement. In the presence of steel rebars inside the pavement, the reflections from the rebars may severely influence the signals reflected from the bottom of the pavement, because metal materials always react stronger to the illuminations of electromagnetic (EM) waves than dielectric materials. In order to make the GPR radar be able to “see” the bottom reflections on real pavement, the following improvements to the GPR hardware were carried out.

2.1 INCREASING GPR’S SAMPLING POINTS

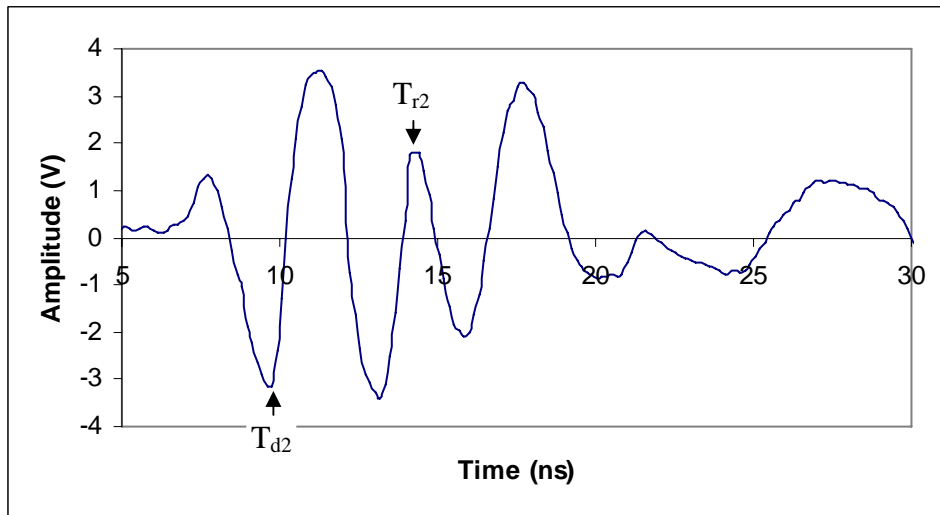
A pulse wave emitted by the GPR radar only has a few nano-seconds (nS) in time duration. Hence the sampling operation to a signal trace has to be carried out within a very narrow time window that is adjusted to focus on the arrival instance of the radar wave. The more points that are sampled for each signal trace, the more details of the signal can be seen (in time dimension), and the higher accuracy of thickness measurement can be obtained. Since the radar can sample only finite points within the time window in each measurement, increasing the sampling points for each sampled trace will surely increase the technical complexity of the GPR radar. In this project, the sampling circuits are modified in order to increase the spatial resolution. The original 256 sampling point is doubled to 512 data points by completely redesigning the sampling circuit and time-delay circuit. [Figure 2.1 \(a\)](#) is one of the waveforms measured over a 10-inch concrete slab using the 512-sampling-point radar. [Figure 2.1 \(b\)](#) is the waveform measured by the 256-sampling-point radar under the same measurement conditions. Carefully comparing [Figure 2.1 \(a\) and \(b\)](#) it can be seen that some high-frequency components are missing in the waveform measured by the 256-sampling-point radar. The measurement error caused by the missing high-frequency components in the above test can be estimated by

$$\frac{|(T_{r2} - T_{d2}) - (T_{r1} - T_{d1})|}{T_{r1} - T_{d1}} = \frac{|4.68 - 4.524|}{4.68} = 3.3\% \quad (2-1)$$

where $T_{r1} - T_{d1}$ is the measured time period that a pulse wave travels forth and back in the concrete slab by the 512-sampling-point radar, and $T_{r2} - T_{d2}$ is the travel time measured by the 256-sampling-point radar. The experiment result illustrates that the measurement accuracy of the improved radar is increased by up to three percent.



(a)



(b)

Figure 2.1 Measured signals using different sampling points, (a) 512 points and (b) 256 points.

2.2 REDUCING DIRECT COUPLINGS

It is common sense that the GPR radar should have a high-power transmitter to reach a deeper penetration, and have a high-gain receiver to receive weak signals reflected from subsurface interfaces. But this design is a two-edged sword. The negative side of the design is that the strong signals from the transmitter can easily couple into the receiver unit through the cables and antennas. The transmitted signals that penetrate into the pavement can provide useful subsurface information, but the signals that directly couple to the receiver unit become strong noises with respect to the subsurface reflections. The noises not only decrease the radar's noise-to-signal ratio, but also disturb the radar's clock signal and interfere with the stability of the receiver. To cut off the paths of direct couplings, all the wires like the common ground lines, power-supply cables and trigger cables should be shielded from passing high-frequency currents. It was found that ferrite materials are especially effective in suppressing high-frequency currents on wires. A series of ferrite tubes are purchased and applied to the cables in the radar system as shown in [Figure 2.2](#). The measured signals before and after the using of the ferrite filters are presented in [Figure 2.3 \(a\) and \(b\)](#). It can be seen that the signal-to-noise ratio of the GPR radar is obviously increased with the use of ferrite filters.

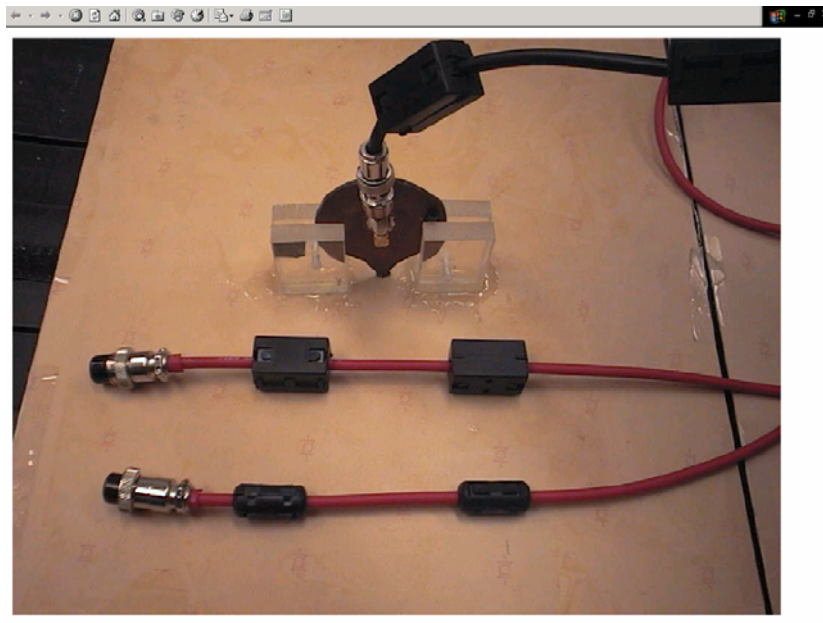
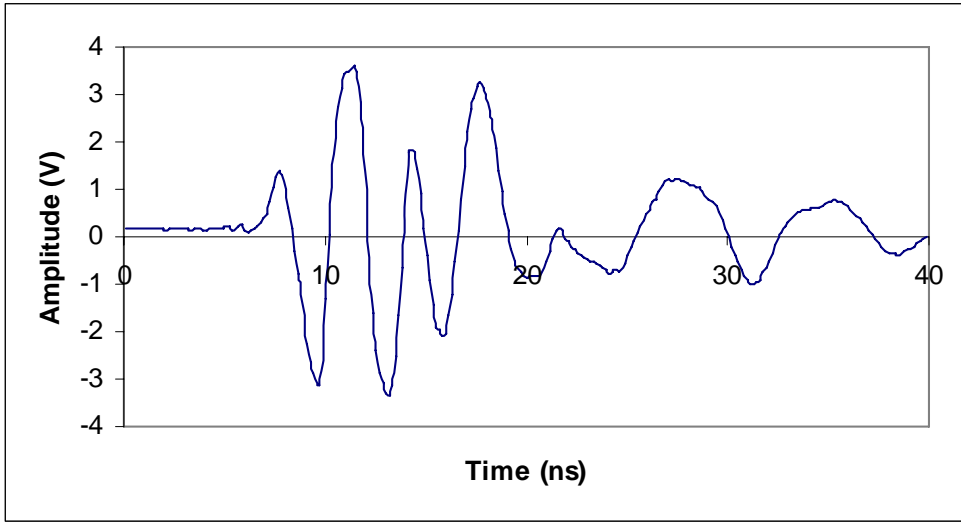
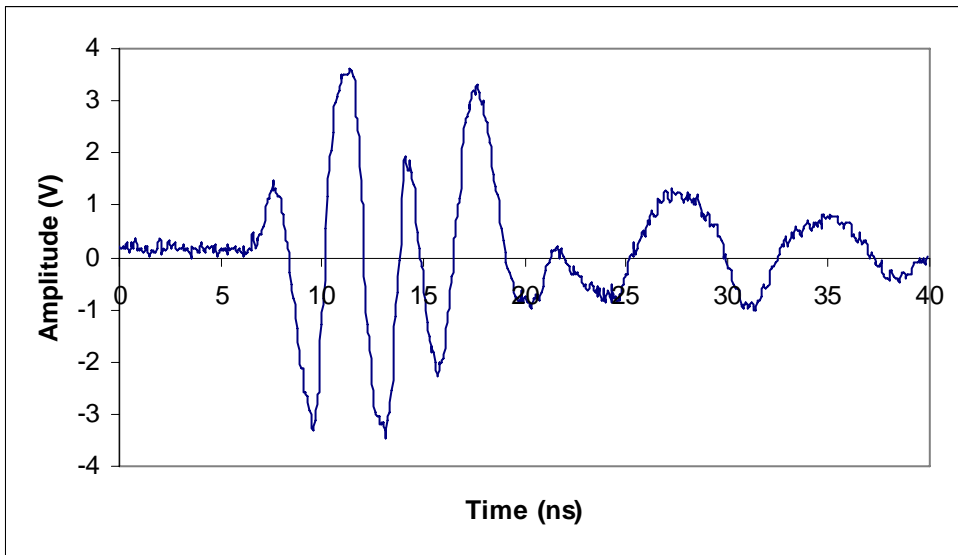


Figure 2.2 Ferrite filters applied on cables



(a)

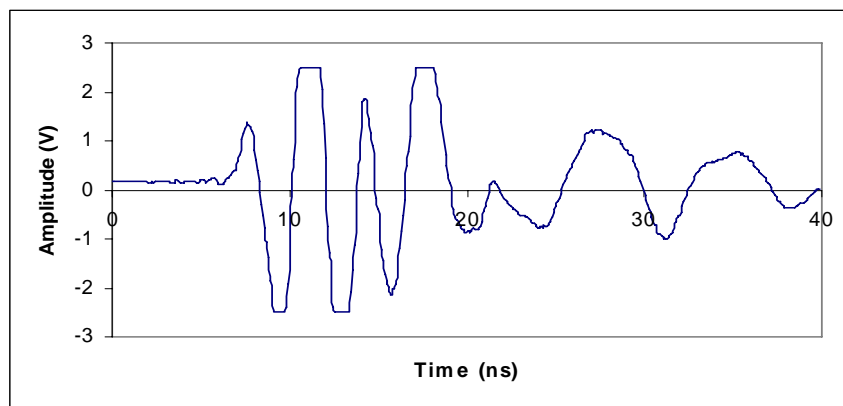


(b)

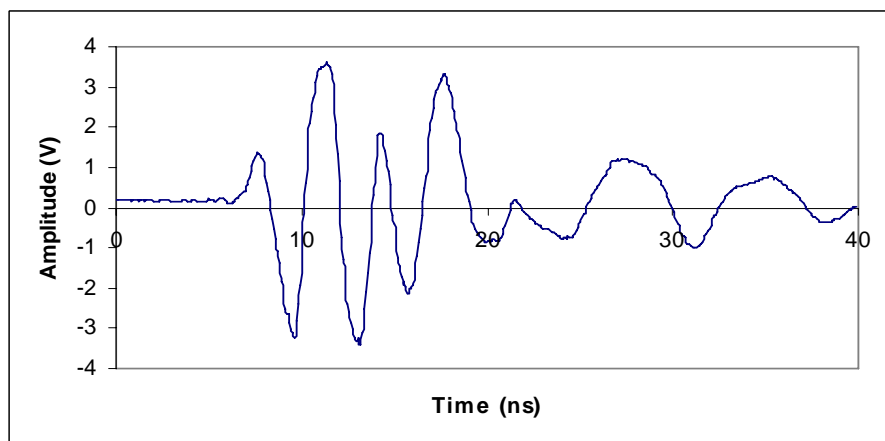
Figure 2.3 Effects of filtering using Ferrite filters, (a) with and (b) without filters

2.3 INCREASING DYNAMIC RANGE

GPR radar is not able to sample signals with any amplitude. Only when the amplitude of the signal falls into a limited range, e.g., -5V to $+5\text{V}$, the signal can then be correctly sampled and recorded by the radar receiver. If part of the signal has the amplitude out of the limited range, this part of the signal will be cut off and the information in this part will be missing. The maximum amplitude range that the radar is able to sample correctly is called dynamic range of the GPR radar. The larger the dynamic range is, the higher resolution the radar can obtain. However, the dynamic range depends on the properties of the electronic components applied and the design of the circuits. In this research, the dynamic range has been improved to $\pm 5\text{V}$ from the original $\pm 2.5\text{V}$. Figure 2.4 shows a measured signal with different dynamic range.



(a)



(b) Figure 2.4 Signals measured by different radar dynamic range, (a) $\pm 2.5\text{ V}$ and (b) $\pm 5.0\text{ V}$

2.4 DISTANCE MEASUREMENTS AND DISPLAY DEVICE

The improved GPR radar can continuously measure the thickness of highway pavements by scanning the radar over the pavement. However, the positions where the traces are obtained have to be recorded manually one by one. In order to make the thickness measurement and the position recording simultaneously and automatically, a distance-measurement device is developed based on an optical shaft encoder. The optical shaft encoder operates by means of a uniformly slotted disk that rotates between a photocell and an LED. When each of the slots on the disk passes in front of the photocell, a light beam from the LED is allowed to pass through the disk and reach the photocell, thus triggering a pulse output. A typical output waveform of the encoder is shown in [Figure 2.5](#).

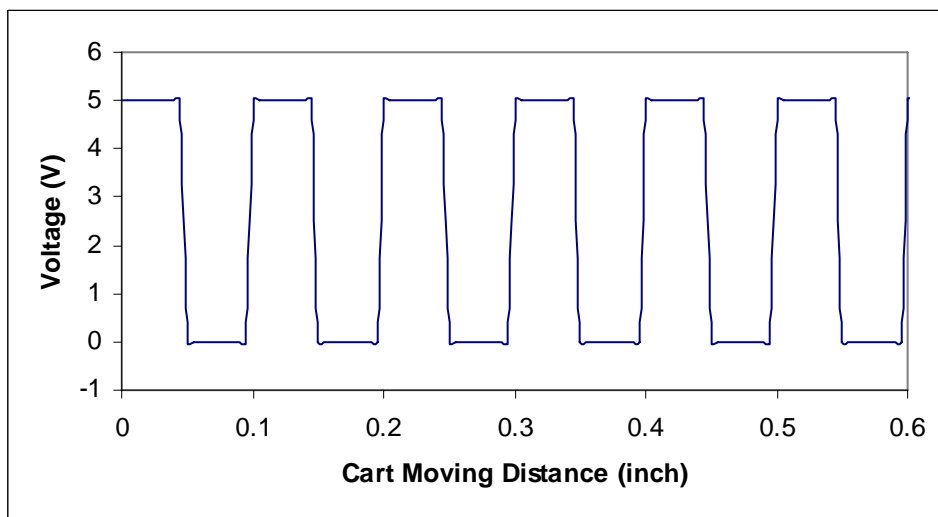


Figure 2.5 Pulses generated by the encoder

The encoder output is directly sent to the computer for processing. If the shaft disk is geared by the cart wheel, N pulses will be generated by the encoder when the cart wheel spins one turn. Here N is the number of the slots on the shaft disk. The distance that the radar cart moves can be calculated by

$$L = \frac{2\pi \cdot n \cdot R}{N} \quad (2-2)$$

where L is the travel distance, R is the radius of the cart wheel, n is the total number of the pulses counted by the computer during the cart movement, and N is the number of pulses that the encoder generates in one wheel turn. As long as the start point of measurement is recorded, all the measurement positions can be determined accordingly.

2.5 LCD DISPLAY

Though the computer monitor is a good device for displaying measured radar data, it is power consuming and not bright enough under strong sunlight. Hence LCD was developed as an alternative displaying device. The LCD screen is about 4.25"×2.75"×2" as shown in Figure 2.6. The communications between the LCD and the control computer are established through the serial port. The travel distance and the measured pavement thickness can be displayed on LCD.

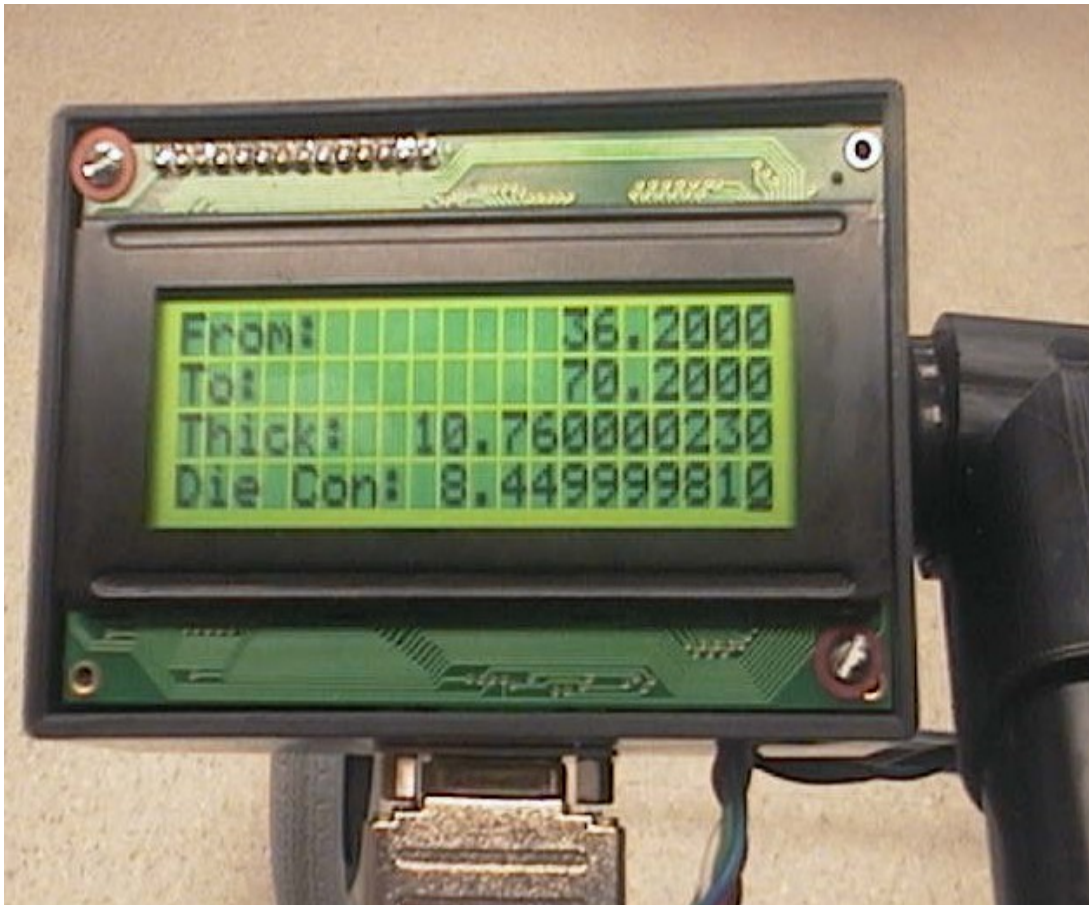


Figure 2.6. The LCD display is clearly seen even under direct sunlight.

The appearance of the improved GPR system is shown in [Figure 2.7](#).



Figure 2.7. The Finalized GPR thickness measurement system

CHAPTER 3: REFLECTED SIGNAL EXTRACTION USING THE SHORT TIME FOURIER TRANSFORM (STFT)

The improvements on hardware significantly increased the signal-to-noise ratio of the radar data. However, there is always a part of the direct wave (feed-through wave from the transmitting antenna to the receiving antenna) arriving at the receiving antenna at the same time as the subsurface reflections. The signals picked up by the receiving antenna are actually a superposition of the direct wave and the subsurface reflected wave. Since the direct wave has much larger amplitude than the reflected wave, special software is needed to extract the reflected wave from the received signal. In this Chapter, STFT is applied to process the measured signals.

3.1 INTRODUCTION TO STFT

Though the standard Fourier Transform is a useful tool for frequency information abstraction, it accounts for the whole time period of the time-domain signal and loses the local temporal information, which is not suitable for the identification of the subsurface reflections. The short-time Fourier Transform (STFT) can not only do spectrum analysis of a time-domain signal as the standard Fourier Transform, but also do it in local time durations, which facilitate the reflected signal analysis.

The STFT of a discrete signal $x(n)$ consisting of N samples is defined as,

$$STFT(n, \omega) = \sum_{m=-\infty}^{+\infty} x(n+m)w(m)e^{-j\omega n} \quad (3.1)$$

In Equation (3.1), $w(m)$ is a real sequence that defines a time window and the signals within this window will be emphasized in STFT computation. The STFT is clearly a function of two variables: the time index number n and the frequency variable ω . For any fixed n , the function $STFT(n, \omega)$ has the same properties as a normal Fourier Transform of a time sequence $x(n+m)w(m)$. It can be interpreted as the Fourier Transform of the signal $x(n+m)$, as viewed through the shifted window

$w(m)$. As n changes, the time window is sliding over the signal along the time axis, and the STFT of the signal can be carried out piecewise along the time axis. In this way, we can get the local information of the signal $X(m)$ at each time index n .

3.2 STFT COMPUTATION

The discrete STFT can be expressed as:

$$STFT(n, k) = \sum_{m=-\infty}^{+\infty} x(n+m)w(m)e^{-j(2\pi/M)km} \quad (3.2)$$

For fixed n , the transform $STFT(n, k)$ is the normal discrete Fourier transform (DFT) of the time sequence $x(n+m)w(m)$. In Equation (3.2), the frequency variable is expressed as k in discrete form, $0 \leq k < M$. The selection of M determines the frequency resolution in STFT. For the GPR system developed above, the sample points in each trace are 512, so we select $M = 1024$. By choosing M as the powers of two, we can take the advantage of FFT (Fast Fourier Transform) algorithm. The primary purpose of using a time window in STFT is to limit the extent of the sequence and emphasize the local features of the measured signals.

3.2.1 VERIFICATION OF THE ALGORITHM

Before the algorithm is used in the project, we use a known data sequence to test the correctness of the algorithm. The data sequence can also be expressed as $\text{noischir}(n) = \cos(\omega_0 n^2) + \text{noise}(n)$. If we do the STFT for $\text{noischir}(n)$, we can get a three dimensional result, time index n , frequency ω , and the spectrum amplitude. Specifying a fixed time index n and carrying out the correspondent Fourier Transform of the sequence $\text{noischir}(n+m)w(m)$, a two-dimensional spectrum graph can be obtained. If we select the frequency with magnitude in the spectrum as the dominating frequency of the signal sequence at the time indexed by n , the dominating frequency should be the base frequency of the signal at the vicinity of time n . In Figure 3.1, the

left chart is the signal $\text{noischir}(n)$, and the right is the dominating frequency chart, where the horizontal axis is time index and the vertical axis is dominating frequency. We can see that the calculated dominating frequency agrees with the theoretical result, except at the very beginning. Because the window is not wide enough, the dominating frequency represents the noise change, not the change of the signal $\cos(\omega_0 n^2)$.

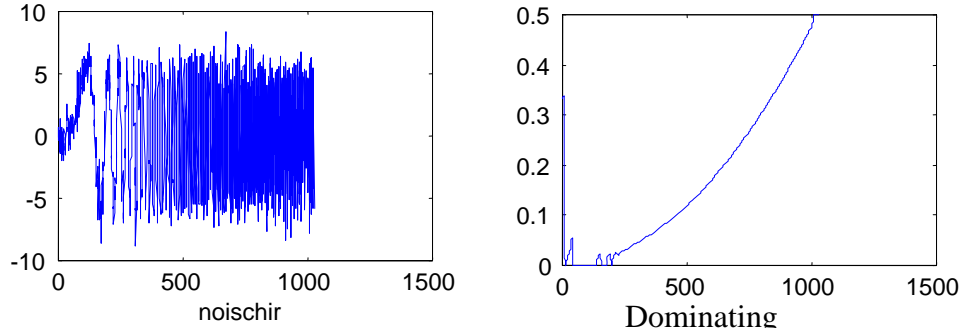


Figure 3.1 Data sequence $\text{noischir}(n)$ and its dominant frequency

3.2.2 WINDOW WIDTH SELECTION

Here we select the window function as $f(i) = e^{-\frac{ci^2}{2}}$; the parameter c determines the window width. A smaller c corresponds to a wider window and a better frequency resolution. On the other hand, a larger c produces a narrower window and a better time resolution. For the example of [Figure 3.1](#), we want to know the dominating frequency at each time n , which is the information in both the time and frequency domain, so the choice of c is the tradeoff between frequency resolution and time resolution. In our application, we are more interested in finding the discontinuously changing point in time domain that may imply the arrival of the subsurface reflections. The frequency information is used as criteria for identifying such changing points. Hence the narrower window can be chosen to get a better time resolution. We will discuss the selection of parameter c through the following examples.

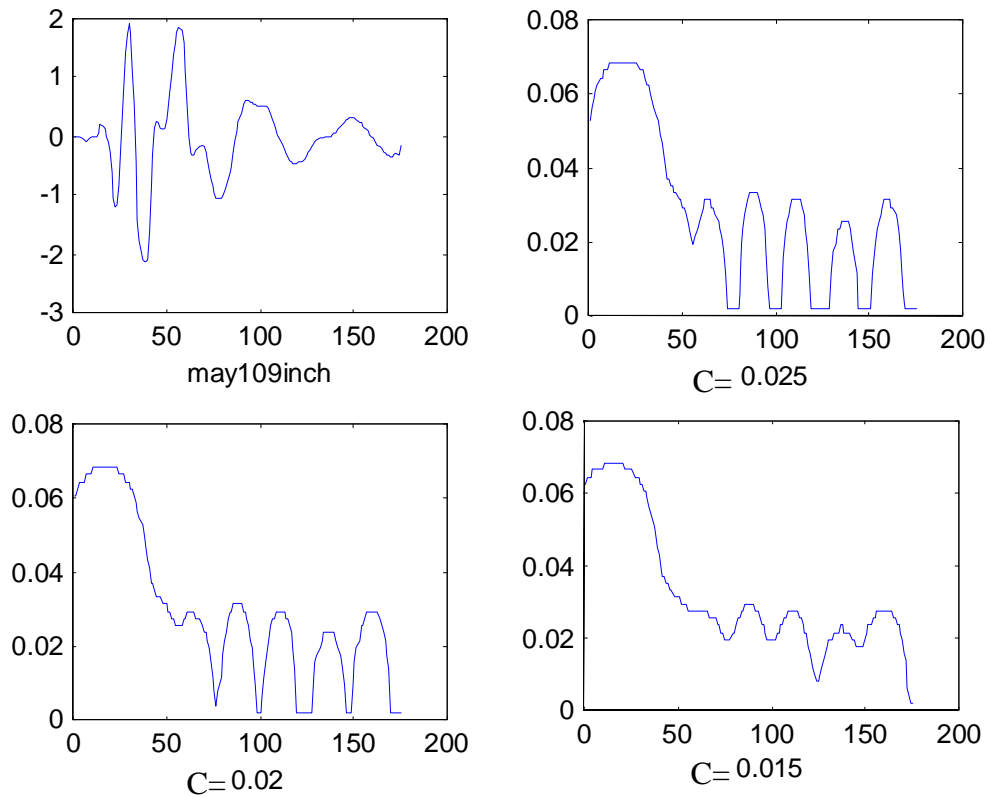


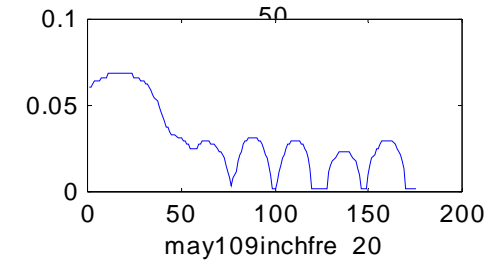
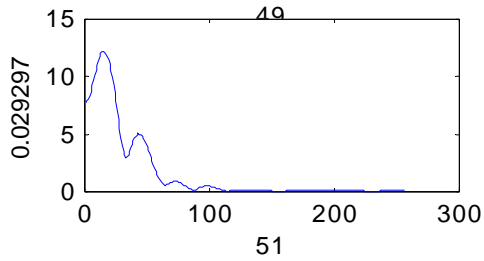
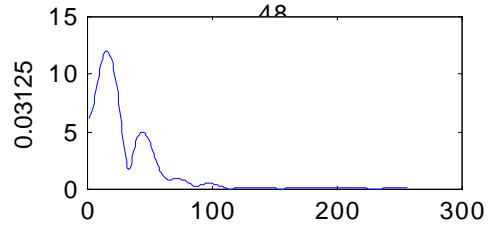
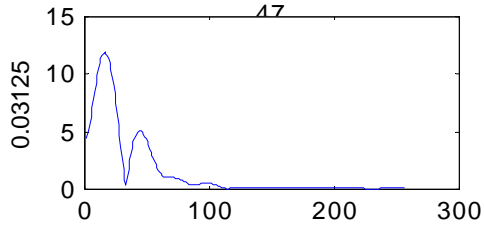
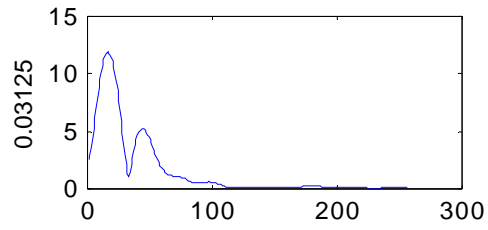
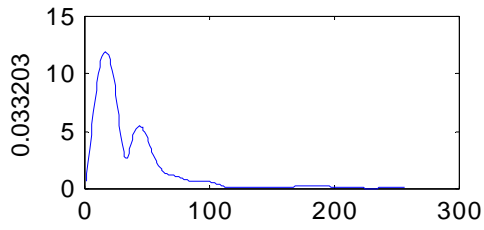
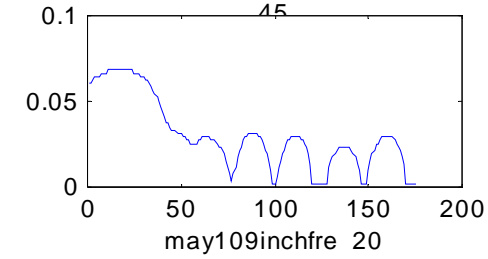
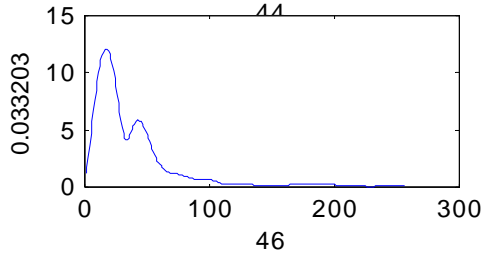
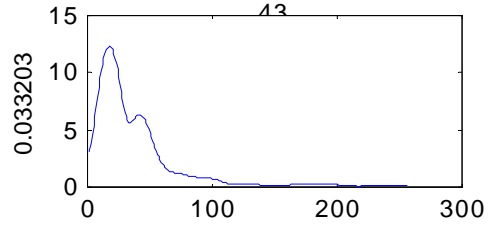
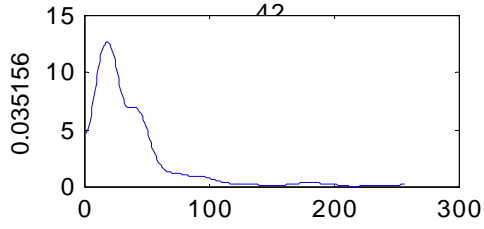
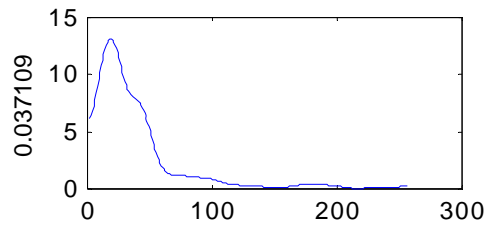
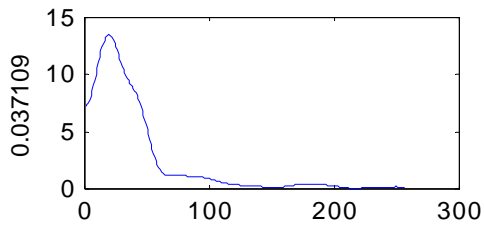
Figure 3.2 The time-domain signal and its dominating frequency at different c , $c=0.015$, 0.02 and 0.025 respectively.

In **Figure 3.2**, the upper left graph is a measured time-domain radar signal. If the STFT of the signal is carried out at each time index number, a series of spectrums can be obtained. The total number of the spectrums is equal to the sampling points of the GPR. In each spectrum we only pick up one frequency that corresponds to the maximum amplitude, then the relationship between the picked-up frequencies and their corresponding time index number can be obtained. The upper right graph is a display of the relationship between the picked-up frequencies and their corresponding time index numbers in the case of $c=0.025$. If we take different values of c and repeat STFT, the bottom two graphs in **Figure 3.2** are obtained. We can see that the choice of $c = 0.015$ makes the frequencies larger than zero at every time point. In the cases of $c = 0.025$, there appear many points with zero-dominant frequency after the time index 75. This is because the window is too narrow and the signal piece within the window is close to a

DC voltage. In this case the time resolution is higher than needed. To get adequate time-domain resolution for the above signal, $c = 0.02$ is verified to be the best choice.

3.3 STFT RESULT ANALYSIS

After we do the STFT for a signal sequence $x[n]$ at each time index number n , we can get a three-dimensional result. The three-dimensional coordinates are composed of time index number, frequency and amplitude. For the sake of convenience, we split the three-dimensional coordinates into a series of two-dimensional graphs. Each two-dimensional graph is a short-time Fourier transform of the sequence $x(n + m)w(m)$ at a given time index number n . In this application, we are interested in finding the feature points on the time-domain signal using the STFT information. The signal shown in [Figure 3.2](#) has a small peak located at the point 50 and it has been verified to correspond to the arrival time of the subsurface reflection by using a metal plate. We carried out the STFT of the signal given in [Figure 3.2](#) at every time point and a few of the STFT results are given in [Figure 3.3](#). It can be seen that two clear peaks appear in the spectrum graph only when the time index number is around the point 50. This result implies that the time-domain signal has two dominant frequencies in the vicinity of the time point 50. In [Figure 3.3](#), the STFT results with the time index from point 42 to point 56 are given.



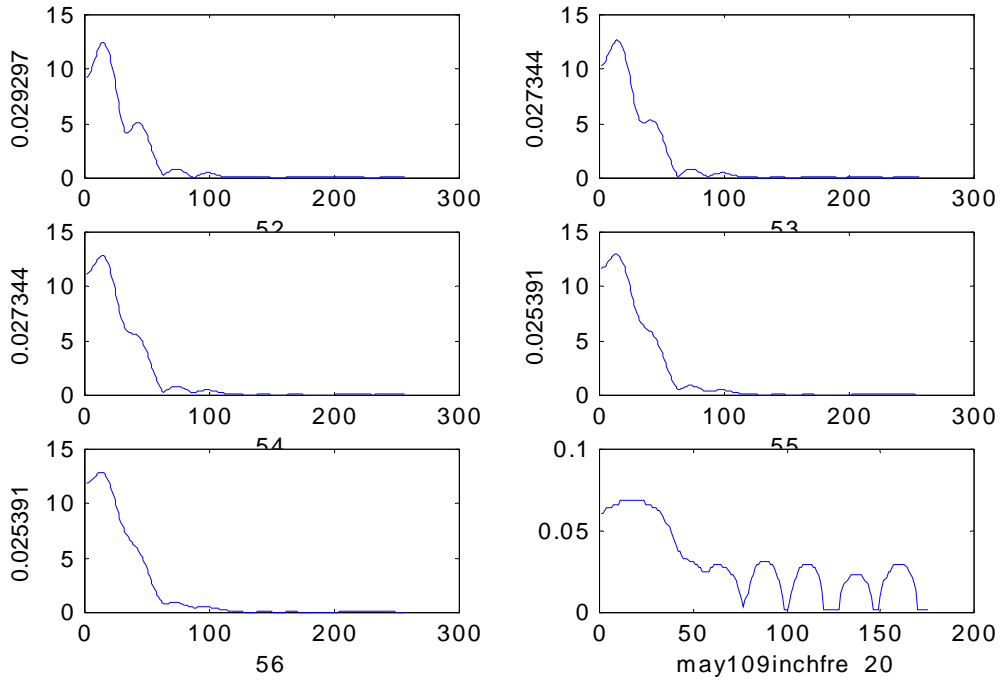
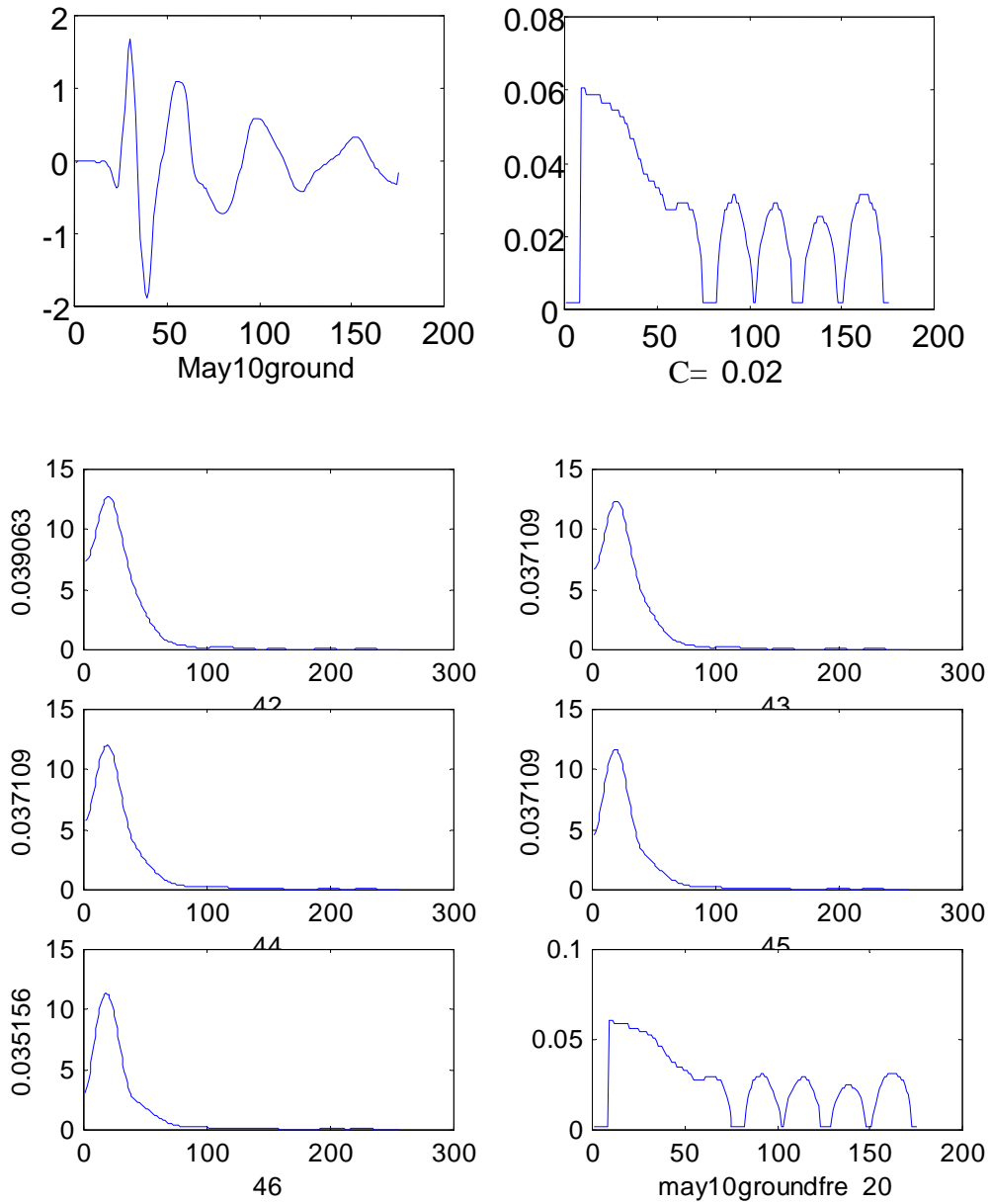


Figure 3.3 STFT results of may109inch.dat from point 42 to point 56

Figure 3.3 demonstrates that the STFT of the radar signal has two clear peaks when the STFT window is in the vicinity of the arrival time of the subsurface reflection. Theoretically, the first peak is the dominant frequency of the base signal and the second peak corresponds to the dominant frequency of the reflected wave, which can be used as a criterion to identify the reflected wave. By combining with the information in time domain, we can accurately locate the arrival time of the subsurface reflections.

This method has been demonstrated to be effective when the reflected wave is strong enough to form a peak on the radar signal. However, in many application cases, the reflected wave can only generate a little discontinuous change on the radar signal instead of forming an obvious peak. For example, for the signal in Figure 3.4, an obvious change can be seen between the deepest valley at time index 39 and the second largest peak at 56 that is caused by the reflected wave. However the reflected wave

does not form a peak on the radar signal between the time indexes 39 to 56 to tell us the exact arrival time of the reflection.



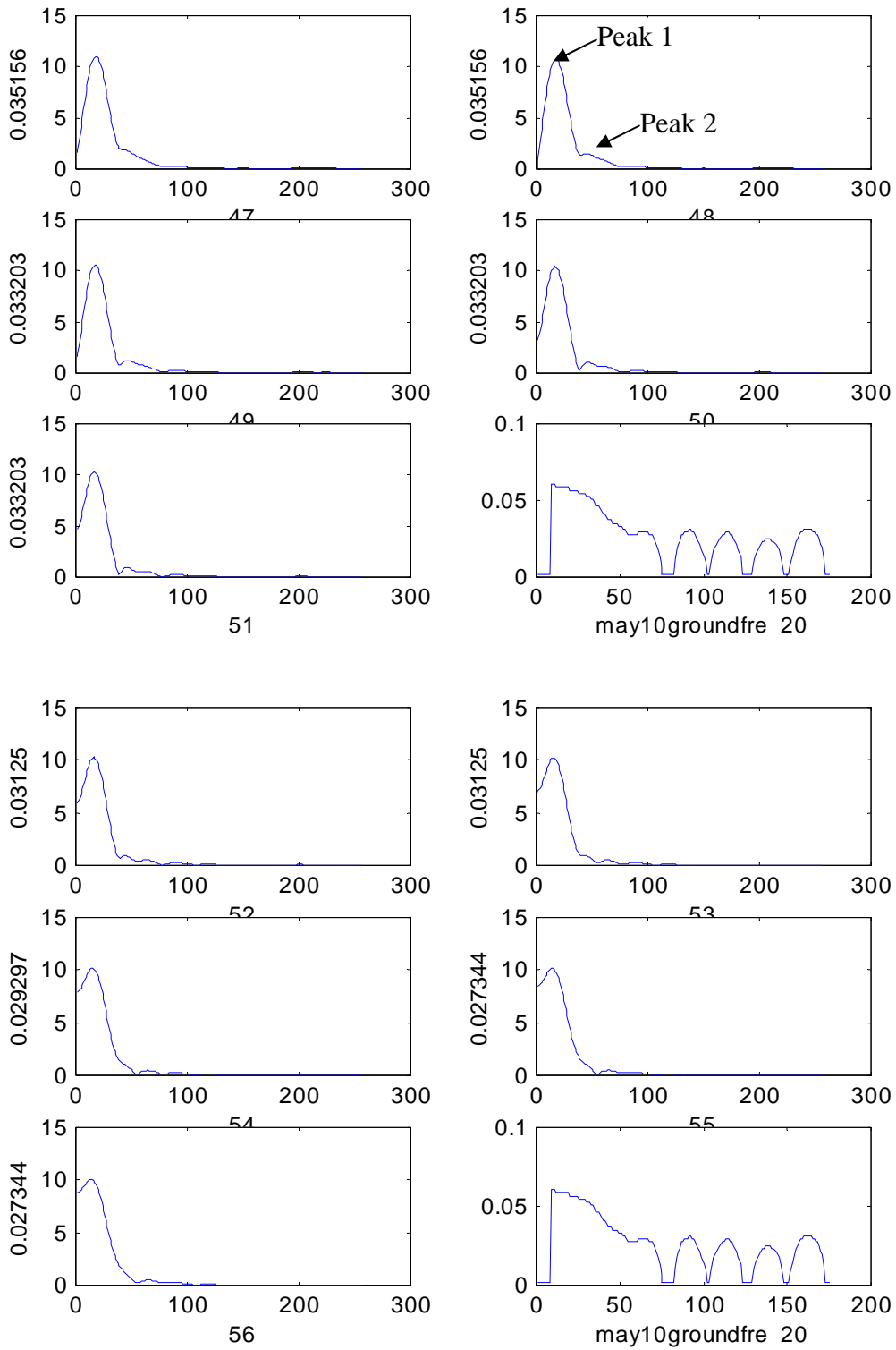


Figure 3.4 STFT results of may10groundfre.dat from point 42 to point 56

From [Figure 3.4](#), we can see that even when the reflection-caused change on the time-domain signal is not obvious, the second peak in the spectrums is still clearly seen though its amplitude is relatively small. Both [Figure 3.3](#) and [Figure 3.4](#) show that as long as a discontinuous change appears on the time-domain signal, the STFT of the signal carried out around the changing point will raise two peaks. This feature of the STFT can be used to justify the arrival of the reflected wave. Since the reflected wave lasts for some time, the two-peak phenomenon appears on several spectrums obtained in the vicinity of the arrival time of the reflected wave, as shown in [Figure 3.3](#) and [Figure 3.4](#). A rule is still needed to determine which spectrum exactly corresponds to the arrival time of the reflected wave. Because the second peak in the STFT spectrum represents the dominant frequency of the reflected wave, the spectrum with the maximum ratio of its second peak over the first peak can be chosen to denote the arrival of the reflected wave, which means the reflected wave reaches its maximum power at that time point.

3.4 APPLICATION PROCEDURES OF STFT

According to the above analysis, the STFT technique can be used to search for the reflected wave and determine the arrival time of it. The application procedures are given below:

- (1) Select the width of the STFT window;
- (2) Carry out the STFT of the signal at each time point;
- (3) Calculate the ratio of the second peak to the first one in spectrum;
- (4) Choose the time point at which the maximum peak-to-peak ratio is obtained.

CHAPTER 4: REBAR PROCESSING

4.1 REBAR'S EFFECTS IN PAVEMENT MEASUREMENT

The electromagnetic response from the rebar-reinforced pavement is quite different from that of plain pavements, because electromagnetic waves are more sensitive to the metal rebar than to the underground dielectric interfaces. It even makes the situation worse that the rebars are located in the middle of the pavement as shown in [Figure 4.1](#) so that the rebar's reflections arrive at the receiving antenna earlier than the reflections from the bottom of the pavement. For the purpose of thickness measuring, the reflections from the pavement bottom are what we need and the rebar reflections are simply noises. Hence the success of the pavement thickness measurement depends on whether we can obtain the signal reflected from the bottom of the pavement and get rid of the rebar reflections.

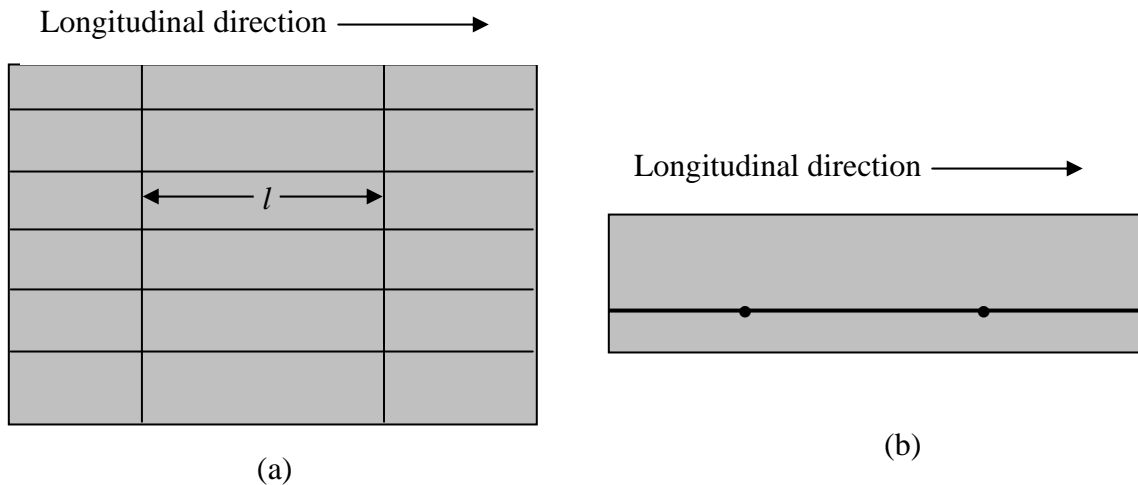


Figure 4.1 Rebar Structure in highway pavement, (a) top view and (b) side view

In order to obtain the reflected signals from the bottom of the pavement and suppress the rebar's reflections, various experiments were carried out to study the effects of rebar quantitatively. Two typical experiments are discussed below.

Experiment 1: the relationship between the rebar's reflection and the polarization of the radar antennas.

A 9-inch-thick concrete slab was used to do the experiment. The slab was set up one inch high above the ground so that a piece of rebar could be easily moved under the slab. When the rebar was orientated in different directions, the rebar's reflections varied a lot. The received amplitude of the rebar's reflections are given in [Table 4.1](#).

Table 4.1 Rebar's reflections in different orientation

Orientation	90°	60°	30°	0°
Amplitude (V)	0.0453	0.3644	0.8187	1.6354

In [Table 4.1](#), 90° corresponds to the perpendicular case shown in [Figure 4.2 \(a\)](#) and 0° corresponds to the parallel case shown in [Figure 4.2 \(b\)](#).

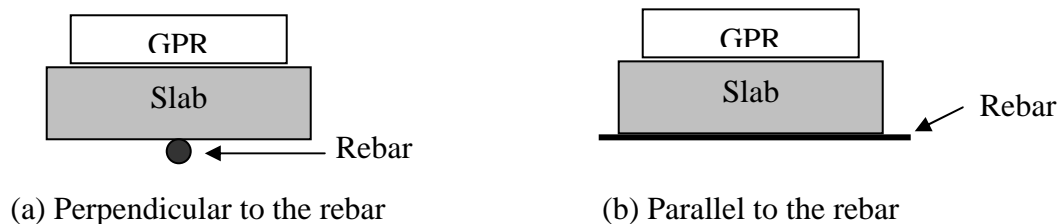


Figure 4.2 Radar's polarization

From the experimental results in [Table 4.1](#), it can be seen that the strength of the rebar's reflection is related to the polarization direction of the radar antennas and the orientation of the rebar. If the radar antennas are polarized in the longitudinal direction of the rebar (0° case), the strongest reflections from the rebar can be received. When the antennas are polarized perpendicular to the rebar (90° case), the rebar's reflections become very weak and can be neglected.

Experiment 2: the relationship between the rebar’s reflection and its relative positions.

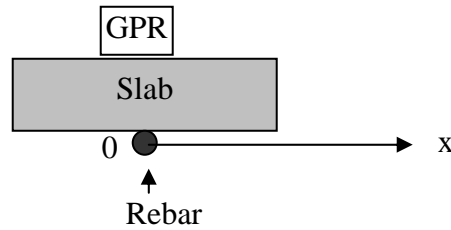


Figure 4.3 Rebar’s reflection versus its relative positions

The measurement system is set up as [Figure 4.3](#). The rebar’s orientation is parallel to the polarization of the GPR radar. When the rebar was moved from the origin 0 in the x-direction, a set of the reflection data was recorded and given in [Table 4.2](#).

Table 4.2 Rebar’s reflections at different positions

Positions (inch)	0	2	4	6	8	10	12
Amplitude (V)	1.63	1.56	1.48	1.22	0.81	0.31	0.034

From [Table 4.2](#), we can see that when the rebar shifted a distance larger than 12 inches in the x-direction, the rebar’s effect can be ignored for practical application.

4.2 MEARING METHODOLOGY ON REBAR-REINFORCED PAVEMENT

For the rebar structure shown in [Figure 4.1 \(a\)](#), if the GPR radar is polarized in the transverse direction and moved in the longitudinal direction with respect to the pavement, the reflection of the rebars orientated in longitudinal direction can be ignored. As long as the space between two transversely orientated rebars is larger than 24 inches, the GPR waves can penetrate the rebar web and reach the bottom the pavement when the radar moves to the the middle place of two adjacent transversely- orientated rebars. Hence there are two requirements to GPR radar when it is used to measure the rebar-reinforced pavement:

- (1) The GPR must polarize perpendicular to the longitudinal direction of the pavement;
- (2) The GPR scans along the the longitudinal direction of the pavement.

Figure 4.4 is a multi-trace chart that was measured on US Highway 59 near Sugarland while the pavement was under construction. This chart contains three-dimensional information. The color represents the signal amplitude, the horizontal axis denotes a trace index that relates to the distance of radar movement, and the vertical axis is the travel time of the GPR waves going down and coming back.

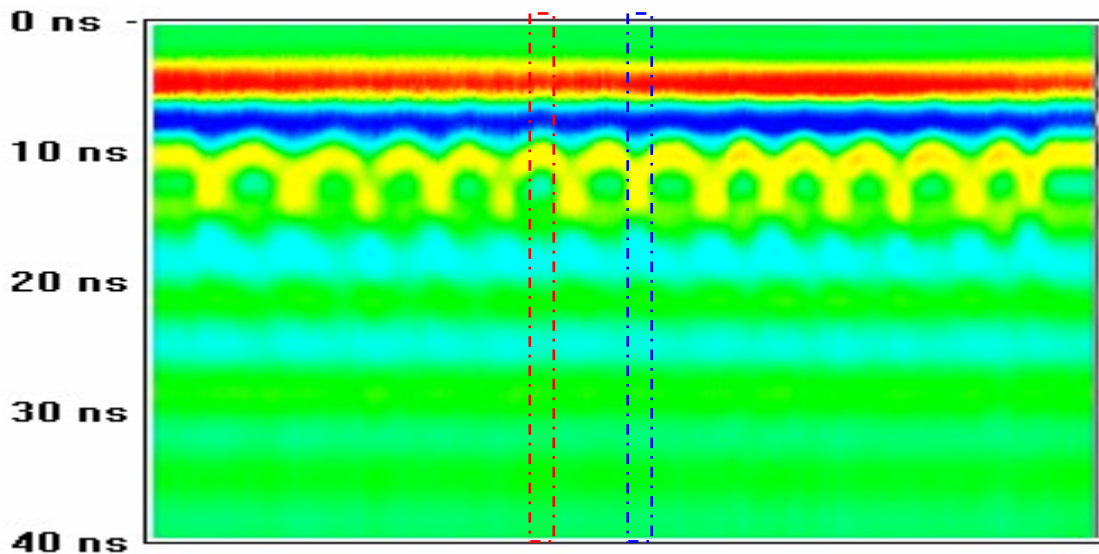


Figure 4.4 Multi-trace chart on highway pavement

The traces are displayed in Figure 4.4 from left to right according to the time order of the trace acquisition. The color pattern in the above chart changes periodically, which corresponds to the subsurface structures. By eye (visually) observing from the side trans-section of the pavement, the traces inside the red-rectangle in Figure 4.4 are recorded while the radar is over a rebar. The traces inside the blue rectangle are recorded at the middle of two transversely orientated rebars. Figure 4.5 gives two typical traces selected from Figure 4.4, one from the red-line-rectangle area and the other from the blue-line-rectangle area.

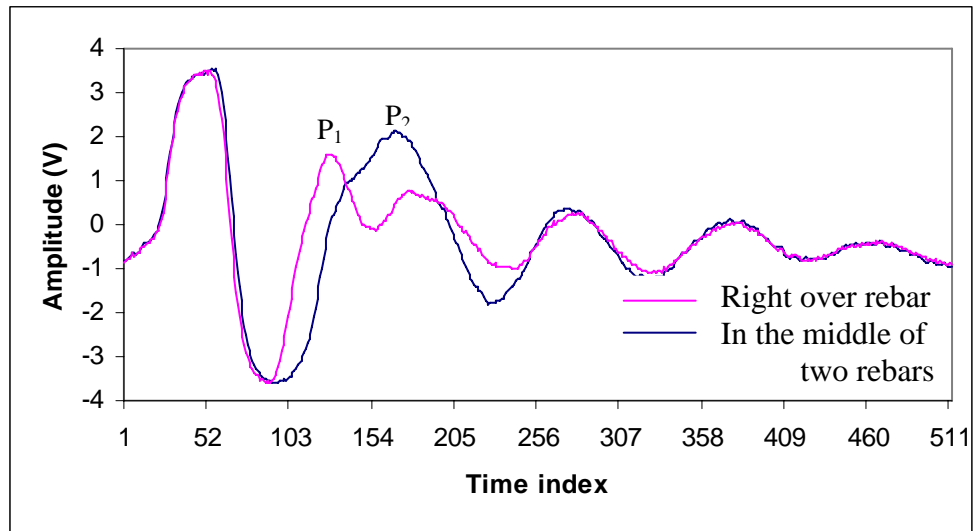


Figure 4.5 Traces measured over and off the rebar

When the radar scans over the pavement, the second largest peak of each graph in [Figure 4.5](#) swings between P_1 and P_2 . The arrival time of rebar reflection and the bottom reflection can be found by the STFT technique.

This page replaces an intentionally blank page in the original.

-- TxDOT Research Library Digitization Team

CHAPTER 5: FIELD MEASUREMENT RESULTS

5.1 MEASURED RESULTS ON HIGHWAY PAVEMENT WITH STEEL REBAR

In January 2002, a field test was carried out on US Highway 59 at Williams Trace in Sugarland. During the measurement, the PD and PI were invited for the field test. [Figure 5.1](#) shows the field condition. The pavement is a new pavement with steel rebar built in.



[Figure 5.1](#). Field test of the developed thickness radar over new pavement with steel rebar (Picture taken by Ed Oshinsky).

Besides the researchers, PD (Dr. Moon Won), PC (Ed Oshinsky), and Dr. German Claros participated in the field test. The field test was done on February 7, 2002 on US Highway 59 North at Williams Trace Boulevard in Sugar Land, Texas. The pavement thickness is an 11-inch concrete reinforced new pavement. GPR thickness

measurement was conducted at the same time with a ruler measurement. In this picture, Dr. Claros measures the pavement thickness using a ruler.

Figure 5.2 shows a cross-sectional view of the concrete pavement tested. The distance between steel rebar in the horizontal direction is about 24 inches.

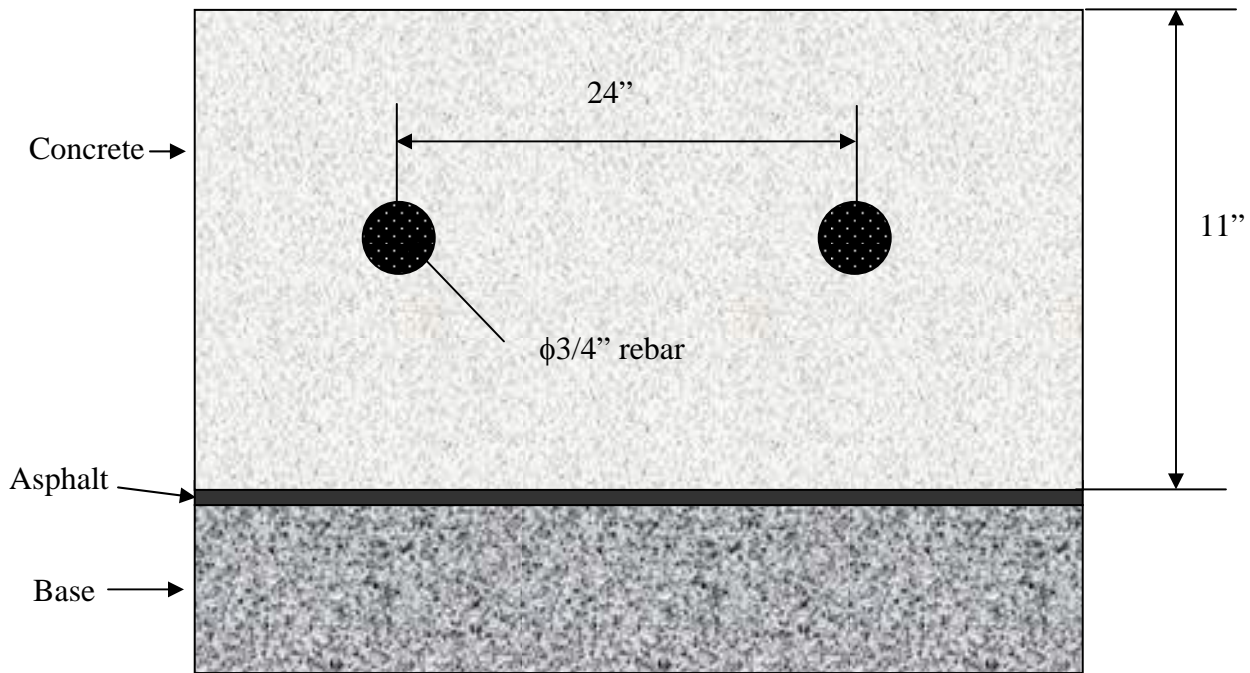


Figure 5.2. Cross sectional view of the concrete pavement used to test the GPR thickness measurement system. Longitudinal rebar is not shown in this figure.

This section of pavement was newly constructed and the border was not yet installed. We were able to measure the thickness using a ruler at the side of the road. During the test, the GPR on the pavement measures a thickness at a point and stores the data. This process is automatic and does not need the operator to input any prior knowledge of the pavement. At the same spot, Dr. Claros measured a thickness using a ruler at the side of the road (as shown in Figure 5.1). One of the recorded GPR images is shown in Figure 5.3. According to the measured traces and the thickness-calculation algorithm described in TxDOT Report #4172, the thickness of the rebar-reinforced pavement can be obtained. The radar-measured thickness results are reported in Figure

5.4. The ruler-measured results are also shown in Figure 5.2 for comparison. In Figure 5.4, the error data is also plotted. Table 5.1 shows statistic data for this test.

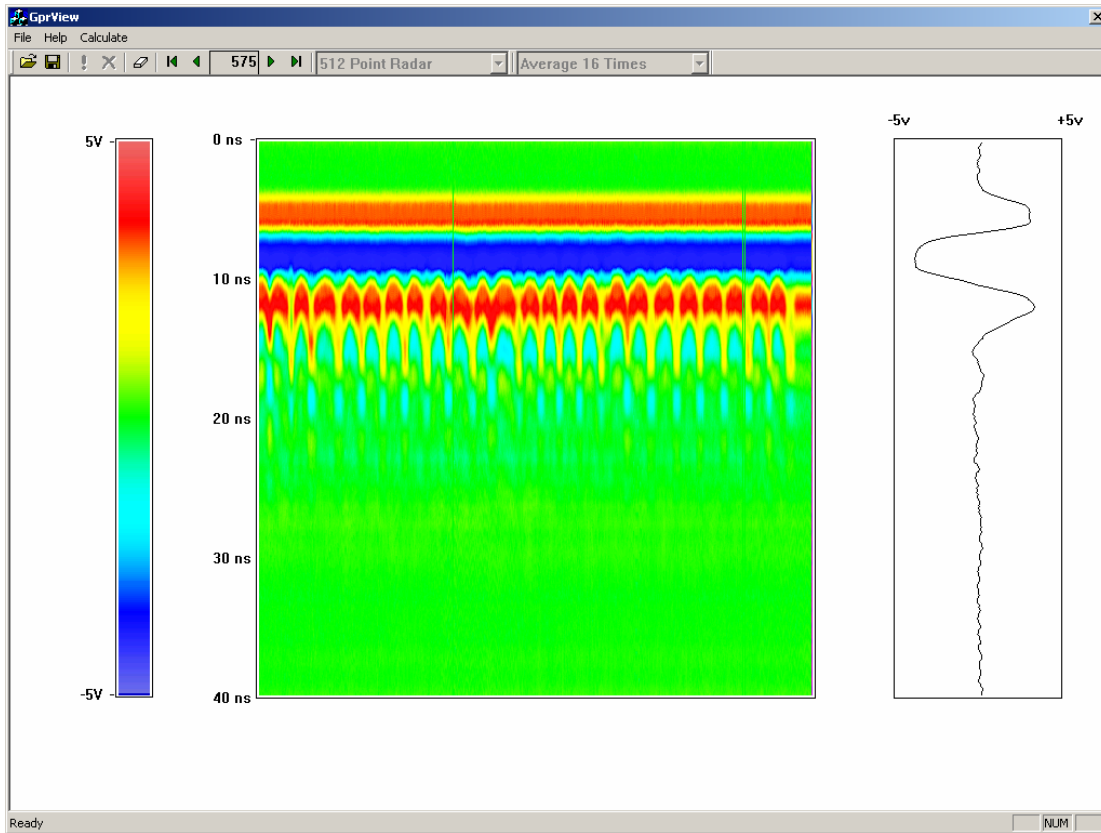


Figure 5.3 GPR image obtained on the pavement during the field test.

Each hyperbola is a signature of a steel rebar. The exact position of the steel rebar is at the top of the hyperbola. The GPR trace showing on the right gives measured waveforms. Most GPR systems require the operator to locate the reflection point on the GPR trace and input the guessed or calibrated dielectric constant to calculate the thickness. In the GPR system developed in this project, the thickness calculation is fully automatic and does not need any prior knowledge of the pavement.

Table 5.1 Average measurement errors by GPR

Average thickness by GPR	Average Thickness by ruler	Average difference	Relative average error
10.82181818	10.60727273	0.214545455	2.0226%

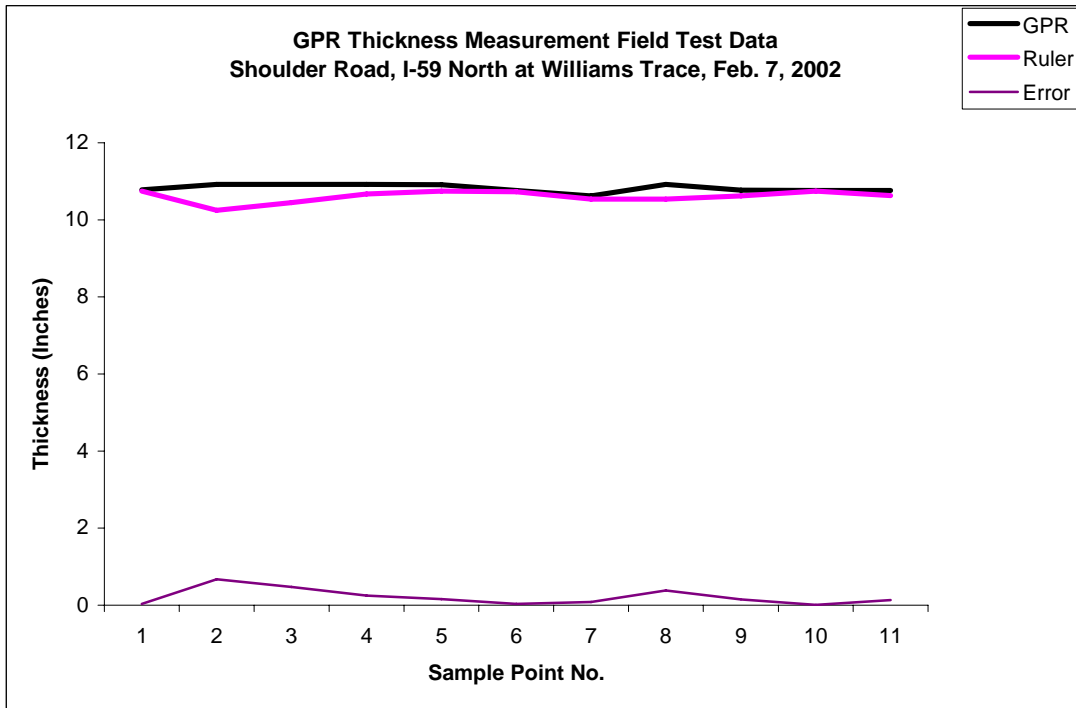


Figure 5.4 Comparison of the radar-measured thickness and ruler-measured thickness

CHAPTER 6: CONCLUSIONS AND RECOMMENDATIONS

6.1 CONCLUSIONS

The improved GPR hardware and software are able to measure concrete thickness automatically with steel rebar in the pavement. The developed GPR thickness radar is a field applicable device that is installed on a pushcart. The entire system is battery operated and is very portable. Field tests on 11-inch pavement showed an average error of 2%.

6.2 RECOMMENDATIONS

1. This thickness measurement radar can be easily implemented for TxDOT's routine pavement thickness monitoring. The cost of this system is very low (less than \$10k each unit). The researchers strongly recommend TxDOT to implement several of these radar units to replace thickness measurement by coring every 1000 feet.
2. The researchers also recommend TxDOT to investigate implementing similar units for vehicle-mount thickness measurement. If so, network-level thickness information can be obtained.
3. The network-level thickness information can be input into PMIS for TxDOT engineers to use in pavement design and maintenance.
4. Similar technology can also be applied to measure asphalt pavement for thickness measurement. Since asphalt pavement is low loss to electromagnetic waves, multi-layer thickness information can be obtained easily. A research in this area is recommended.
5. We also recommend further development of the automatic thickness computation algorithm so that it can be applied to multi-layer cases.
6. The thickness radar also extracts the dielectric constant of the concrete. Therefore, the moisture content of the pavement can be obtained because of the strong dependence of the dielectric constant with the moisture content of the

pavement. Currently, this information is not being used. Further study on the relationship between the moisture content in concrete and dielectric constant is recommended.